Supplementary information for

Resolving quinoid structure in poly-para-phenylene chains

Bingkai Yuan[1, ‡], Can Li[1, ‡], Yan Zhao[1], Oliver Groning[2], Xieyu Zhou[3], Pengfei Zhang[4], DanDan Guan[1,6], Yaoyi Li[1,6], Hao Zheng[1,6], Canhua Liu[1,6], Yiyong Mai[4], Peinian Liu[5], Wei Ji[3], Jinfeng Jia[1,6], Shiyong Wang[1,6]*

[1]Key Laboratory of Artificial Structures and Quantum Control (Ministry of Education), Shenyang National Laboratory for Materials Science, School of Physics and Astronomy, Shanghai Jiao Tong University, Shanghai 200240, China

[2]Empa, Swiss Federal Laboratories for Materials Science and Technology, 8600 Dübendorf, Switzerland

[3]Department of Physics, Renming University, Beijing 100872, China.

[4]School of Chemistry and Chemical Engineering, Shanghai Jiao Tong University, Shanghai 200240, China

[5]Shanghai Key Laboratory of Functional Materials Chemistry, East China University of Science & Technology, 130 Meilong Road, Shanghai, 200237, China

[6]Tsung-Dao Lee Institute, Shanghai Jiao Tong University, Shanghai, 200240, China.

KEYWORDS: Quinoid, Poly-para-phenylene, On-surface synthesis, Nc-AFM, STM, In-gap states

*Corresponding Author**: shiyong.wang@sjtu.edu.cn

‡These authors contributed equally.

Contents:

Experimental and calculation details:

Experiments

   All the experiments were carried out in a commercial ultra-high vacuum low-temperature Joule-Thomson scanning probe microscope (Unisoku) with a Nanonis control system. The Cu(111) single crystal was cleaned by repeated cycles of sputtering and annealing. DBTP molecular precursors (jkchemical, 95%) were evaporated onto Cu(111) held at the temperature between 448 K-513 K. CO molecules were in situ dosed into sample held at around 7 K through a leak valve with a typical pressure of 5×10^{-9} mbar for 1 minute. CO-functionalized tips were prepared by picking up CO molecules from NaCl islands on Cu(111). STM and AFM images were acquired at 5K. The bias voltages referred to the sample in both STM and AFM images. The STM images were recorded in constant-current mode and the dI/dV spectra were recorded using a lock-in technique (U_{RMS} = 20 mV). The AFM images were recorded in constant-height frequency modulation mode (resonance frequency 25 kHz, quality factor about 20000) with CO-functionalized tip.

Tight binding calculations

   The tight binding (TB) calculation of the STM images were carried out in the C $2p_z$-orbital description by numerically solving the tight-binding Hamiltonian with nearest-neighbor hopping:

$$\widehat{H} = \sum_{<ij>} -t_{ij} c_i^+ c_j^-$$

with t_{ij} is the nearest-neighbor hopping term depending on the bond length between C atoms[1,2] (t_{ij}(-2.07eV) and t_{ij}(-3.3eV) correspond to C-C single bond and double bond with bond length 0.154nm and 0.133nm respectively) and c_i^+ and c_j^- denoting the creation and annihilation operators of $2p_z$-electron on the atomic site i and j. Numerically solving the model Hamiltonian yields the energy Eigenvalues E_i and the corresponding Eigenstates $\alpha_{i,j}$ (amplitude of state i on site j) from which the wave functions are computed assuming Slater type atomic orbitals:

$$\psi_i(\vec{r}) = \sum_j \alpha_{i,j} \cdot (z - z_j) \exp\left(-\zeta|\vec{r} - \vec{r_j}|\right)$$

with $\zeta = 1.625$ a.u. for the carbon $2p_z$ orbital. The charge density map $\rho(x,y)$ for a given energy range $[\varepsilon_{min}, \varepsilon_{max}]$ and height z_0 is then obtained by summing up the squared wave functions in this chosen energy range.

$$\rho(x,y) = \sum_{i,\varepsilon_i \in [\varepsilon_{min}, \varepsilon_{max}]} \psi_i^2(x, y, z_0)$$

Constant charge density maps are taken as a first approximation to compare with experimental STM images.

Density functional theory calculations

Our density functional theory calculations were performed using the generalized gradient approximation and the projector augmented wave method[3,4] as implemented in the Vienna ab-initio simulation package (VASP)[5,6]. Dispersion correction, which considers van der Waals interactions, was employed with revised Perdew-Burke-Ernzerhof functional (RPBE-Δ_3)[7,8]. An orthorhombic $2\sqrt{3} \times 5$ supercell consisting of 120 Cu atoms in six layers with at least 15 Å vacuum region, was employed to model the benzenoid chain adsorbed on Cu (111) surface. The benzenoid chain contains 12 C atoms and 8 H atoms, which have periodicity in **a** direction. The uniform Monkhorst-Pack k mesh of $6\times4\times1$ was adopted for integration over the 2D surface Brillouin zone. A plane-wave cutoff energy of 400 eV was used for structural relaxation and electronic structures. All atoms except the bottom three Cu layers were allowed to relax until the residual force per atom was less than 0.02 eV/ Å. Hole doping on C atoms was used to simulate the effects of losing H atom. The charge doping on C atoms was realized with ionic potential method[9,10]. For hole doping, electrons were removed from the valence band by adding a negative potential into the 1s core level of C. The dipole correction was also considered in this asymmetric slab model.
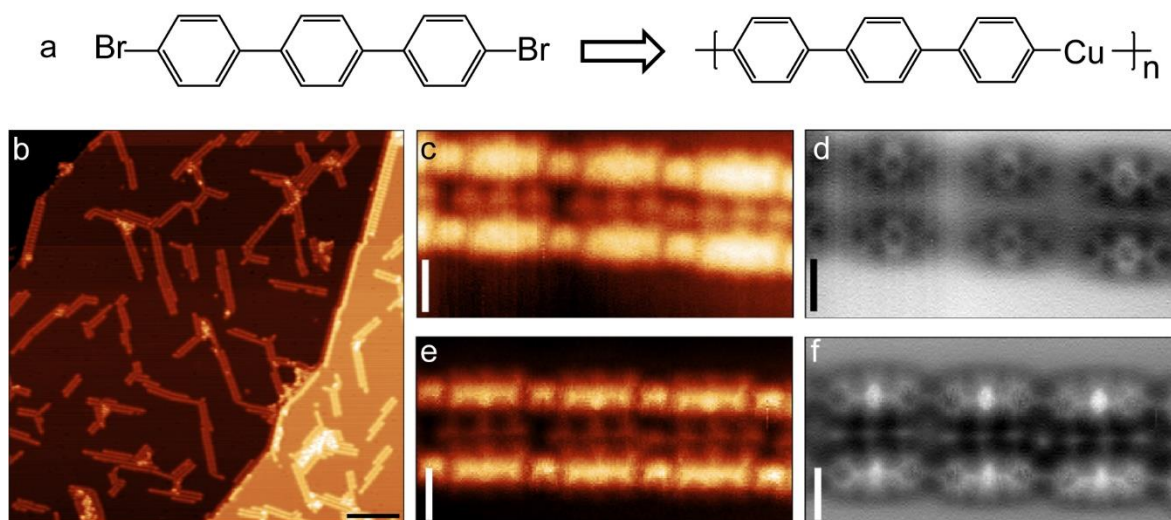
Figure S1. Structural properties of organometallic intermediate. a. Reaction scheme from 4,4''-dibromo-p-terphenyl mono-
mers to Cu-(ph)$_3$-Cu intermediate. **b**. Overview STM image of organometallic intermediate fabricated on a Cu(111) surface at
room temperature (Bias: 1 V, Current: 20 pA; Scale bar: 5 nm). **c and d**. Zoom-in constant-height current and nc-AFM images
of organometallic intermediate (Bias: 1mV; Oscillation amplitude: 50 pm; Scale bar: 1 nm). **e and f**. Zoom-in constant-height
current and nc-AFM images (Bias: 1mV; Oscillation amplitude: 50 pm; Scale bar: 1 nm) of organometallic intermediate with tip-
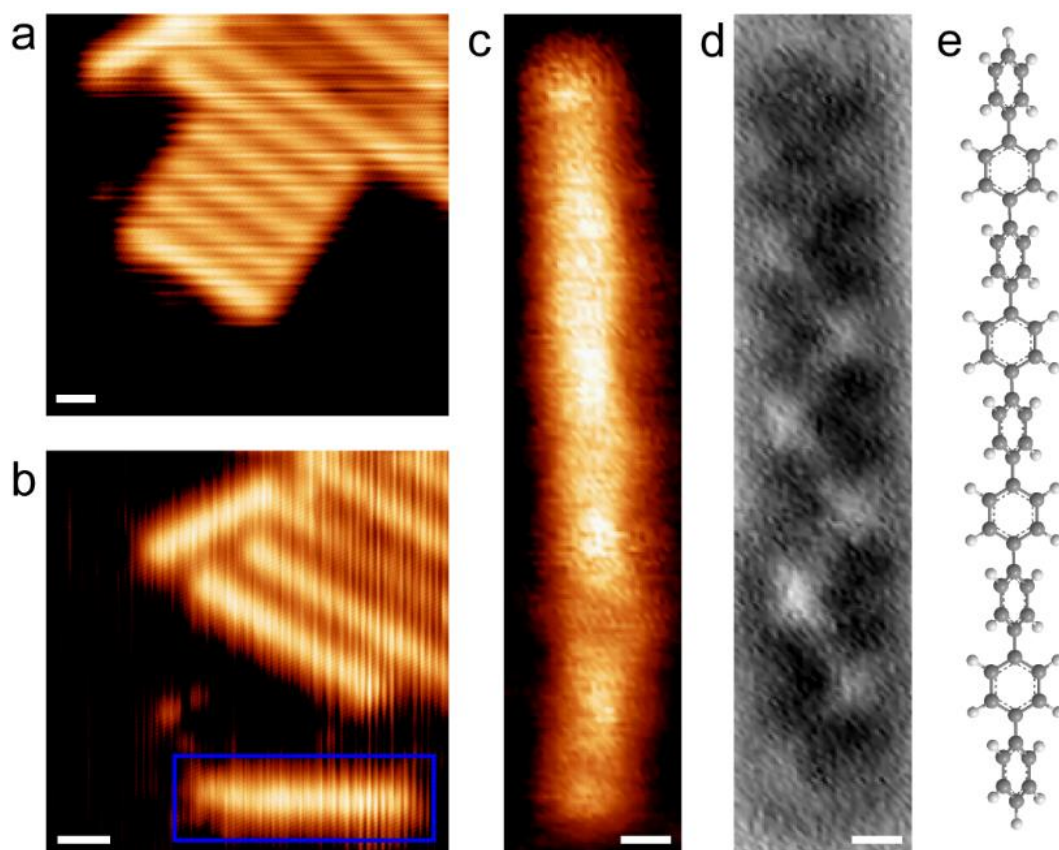sample distance reduced by 0.2 Å with respect to **d**.

Figure S2. STM manipulation of PPP chains out of an island. a and b. STM images before and after the manipulation (Bias: 0.5 V, Current: 20 pA). **c-e.** Current image, nc-AFM image and chemical model of the benzenoid PPP chain marked with blue rectangle in **b**. This chain hosts a twisted structure after dragged out from the island, indicating a non-planer benzenoid structure. The scale bars in **a** and **b** are 1.0 nm; The scale bars in **c** and **d** are 0.25 nm.
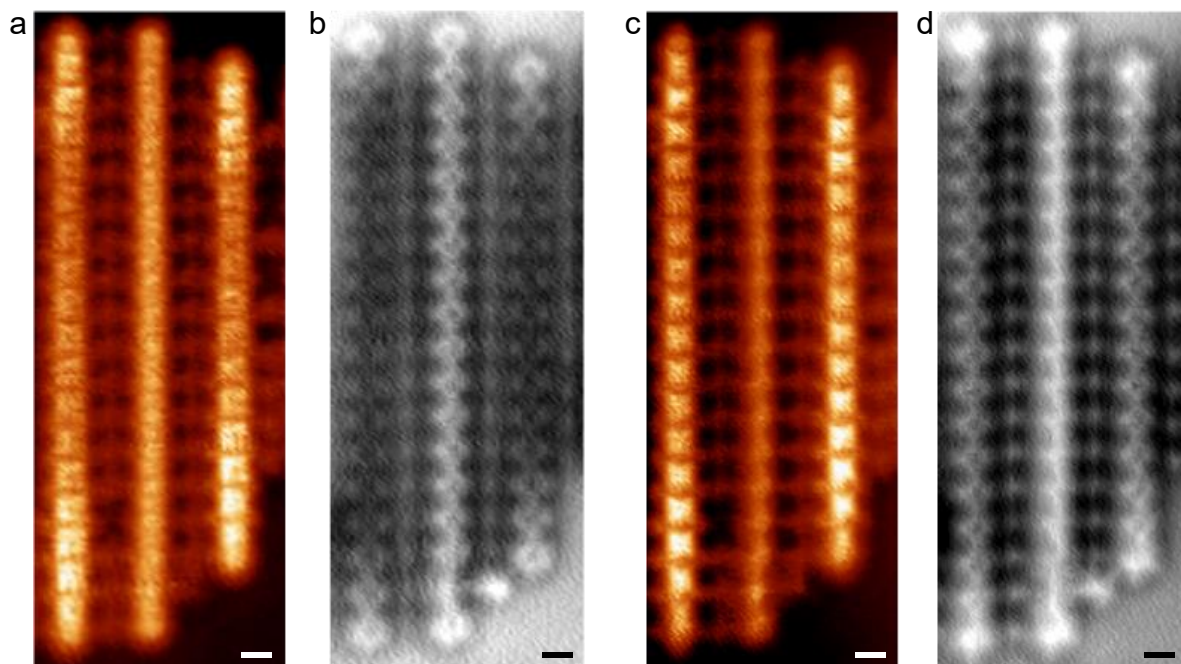
Figure S3. Current and nc-AFM images of PPP chains taken at different tip-sample heights. a and b. Current image and nc-AFM image of one quinoid chain and two benzenoid chains. The two side bonds of quinoid rings show pronounced frequency-shift intensity. **c and d.** Current image and nc-AFM image taken at closer tip-sample height than that in **a and b**. Quinoid rings exhibit similar bond contrast as benzenoid rings in **b**, suggesting that quinoid rings adsorb closer to the surface than that of benzenoid rings. Scale bars: 0.5 nm. Bias voltage: 1 mV.
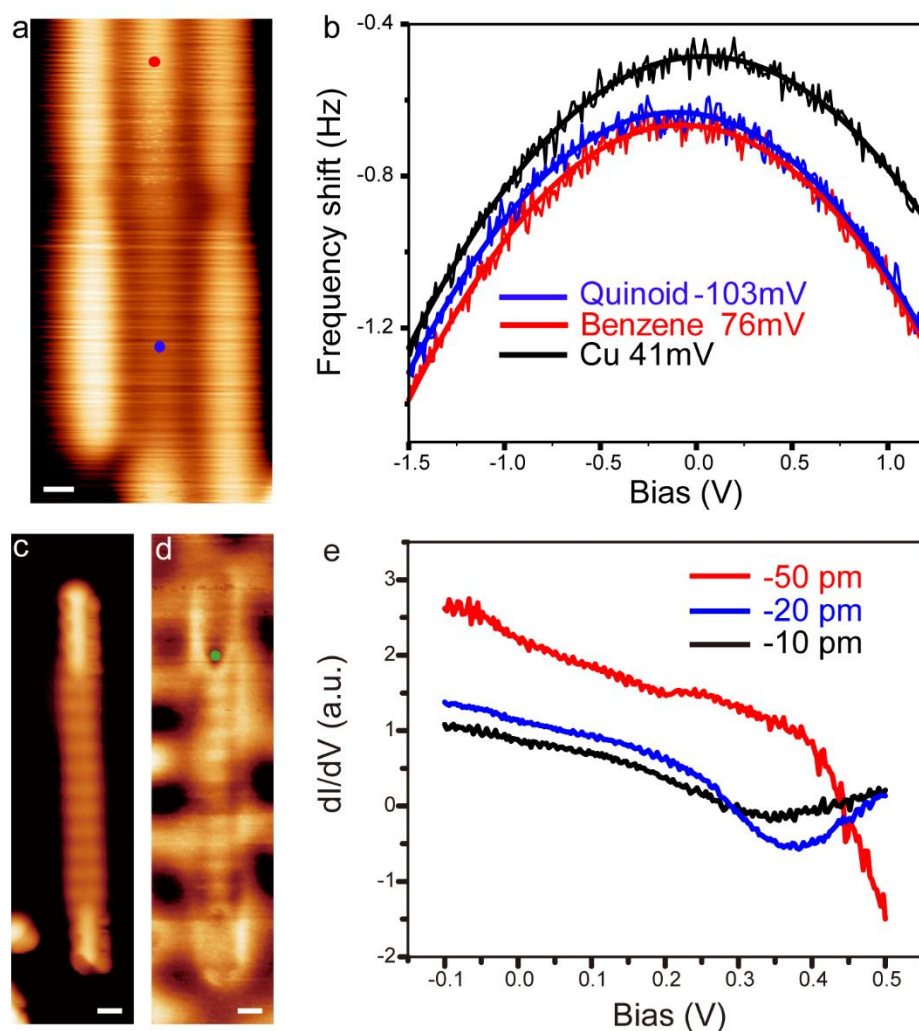
Figure S4. Charging states of quinoid structure. a. STM image (Bias: 1.0 V, Current: 10 pA) showing one quinoid chain and two benzenoid chains. **b.** $\Delta f(V)$ spectra recorded on top of benzenoid, quinoid and Cu(111) surface. The local contact potential difference (LCPD) can be distracted by fitting the df(V) parabolas. The LCPD between the Cu/benzenoid/quinoid and the tip are 41 mV/-76 mV/-103 mV, respectively. The negative LCPD on quinoid chains indicates a hole doping from substrate. **c-d**. STM image and dI/dV mapping (Bias: -0.1 V, Current: 200 pA) of a single quinoid chain. **e**. dI/dV spectra taken at the interface at different tip-sample heights. As the tip gets closer, the position of the dip shift to more positive bias, indicating the existence of a localized positive charge at interfaces. dI/dV spectra are taken at the interface as marked by the green dot in **d**. Scale bars: 0.5 nm.

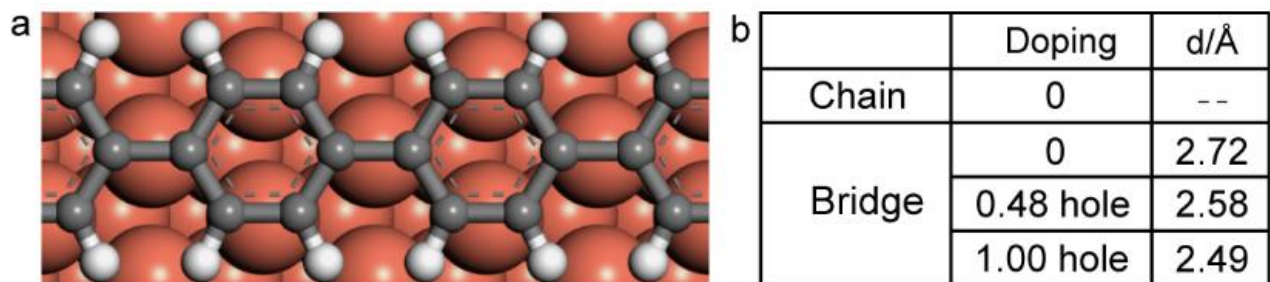|		Doping	d/Å
Chain		0	--
Bridge		0	2.72
		0.48 hole	2.58
		1.00 hole	2.49

Figure S5. DFT optimized adsorption configuration of PPP on Cu(111). a. Optimized adsorption configuration of PPP on Cu(111). **b**. Adsorption height as a function of hole-doping level from the substrate. Delocalized hole doping is considered in DFT calculations. PPP chains with higher hole doping level adsorb closer to Cu(111), in support of the observed lower adsorption height of quinoid segments due to hole doping.
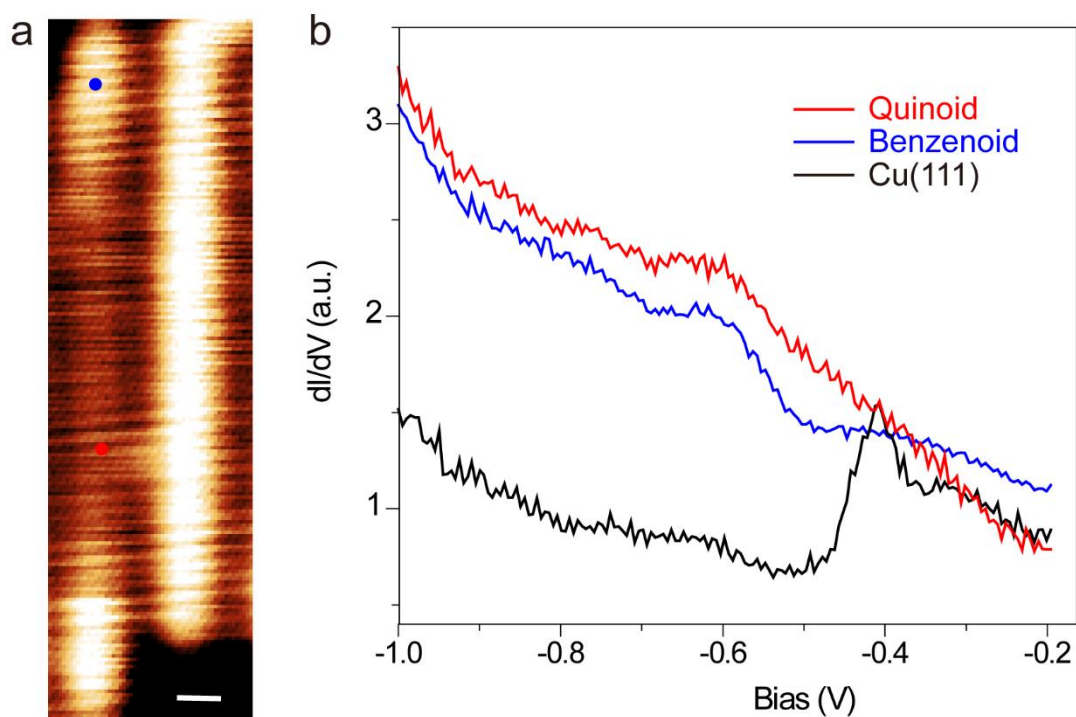
Figure S6. Resolving the occupied states of quinoid PPP. a. STM image (Bias: 1 V, Current: 10 pA; Scale bar: 0.5 nm) showing a quinoid and a benzenoid PPP chain. **b**. dI/dV spectra with large tunneling current setpoint taken at the positions marked by colored dots in a. The black curve was taken at nearby Cu surface for reference. The highest occupied band onset is resolved in dI/dV spectra, showing a enhanced LDOS intensity at -0.6 V.
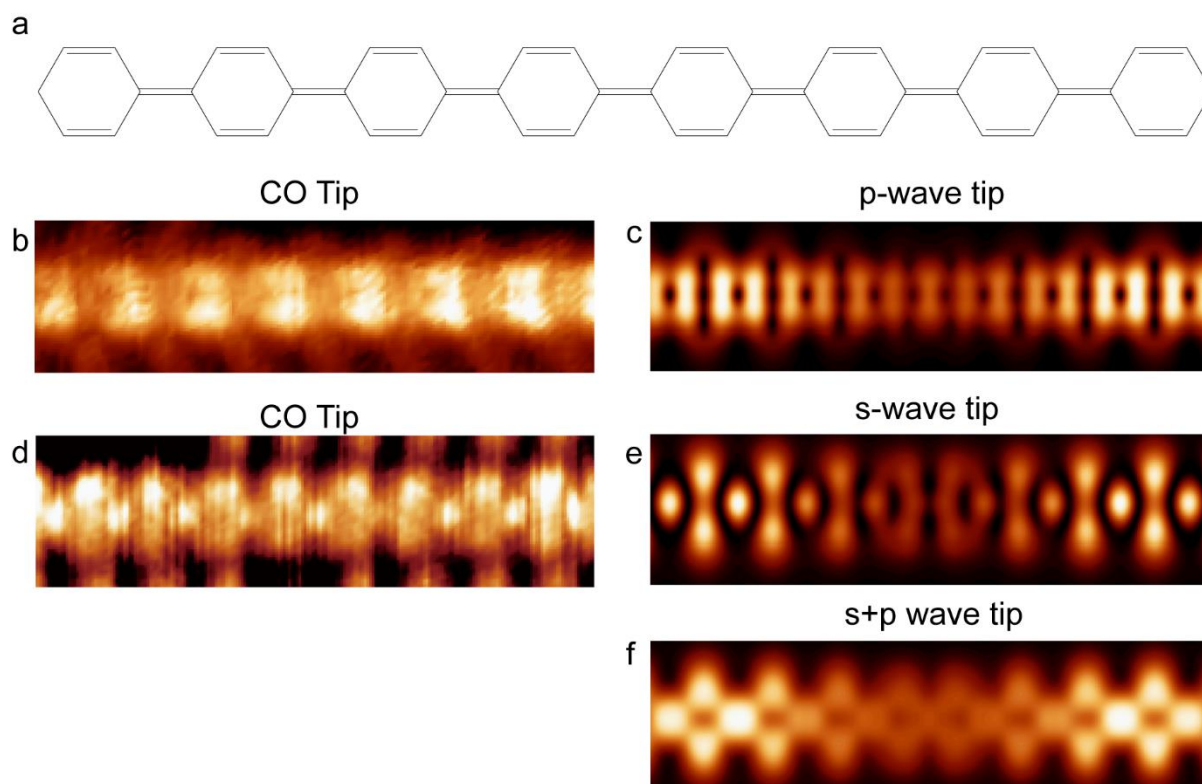
Figure S7. Current images of quinoid structure taken with different tips. a. Chemical structure of quinoid structure. **b-c.** Current image of quinoid structure using CO-functionalized tip and the corresponding simulated LDOS image with a *p*-wave tip. **d-f.** Current image of quinoid PPP using a different CO tip and the corresponding simulated LDOS images with a pure *s*-wave tip and a mixed *s+p* (ratio s/p=4:1) tip.
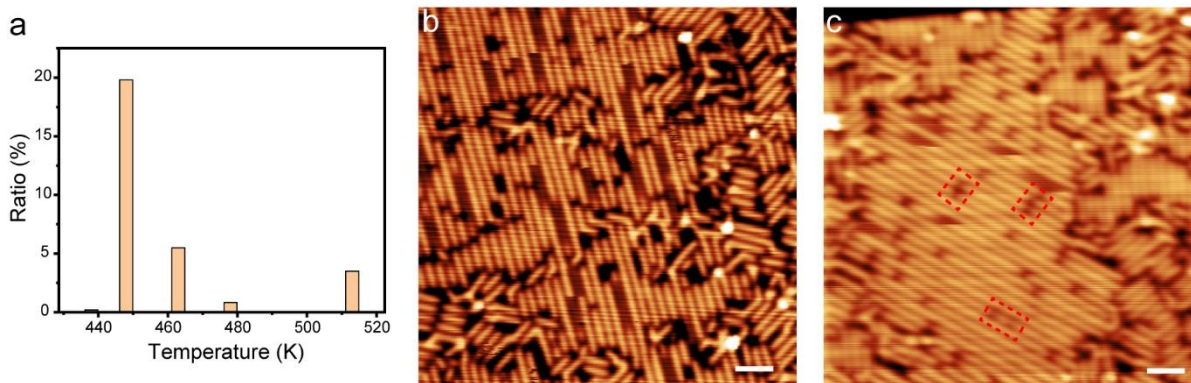
Figure S8. Ratio of quinoid chains as a function of annealing temperature. a. Ratio of quinoid segments after annealing the same sample to different temperatures. The amount of quinoid segments increases with the annealing and reach a maximum population of 20% at 448K, then decreases rapidly after annealing to even higher temperatures. **b.** The typical STM image (Bias: 1 V, Current: 20 pA) after annealing at 448K for 20min. The ratio of quinoid segments is 20%. Some PPP chains undergo dehydrogenation reaction at elevated temperature and the missing hydrogen atoms create radicals, facilitating benzenoid-to-quinoid transitions. **c.** A typical STM image (Bias: 1 V, Current: 10 pA) after annealing at 478K for 20min. The ratio of quinoid segments decreases quickly to 0.83%. The quenching of quinoid at even higher temperature is due to the formation of bonds between radicals and substrate, exhibiting as short dark contrast in STM images as marked by red dashed rectangles. Scale bars: 4nm.
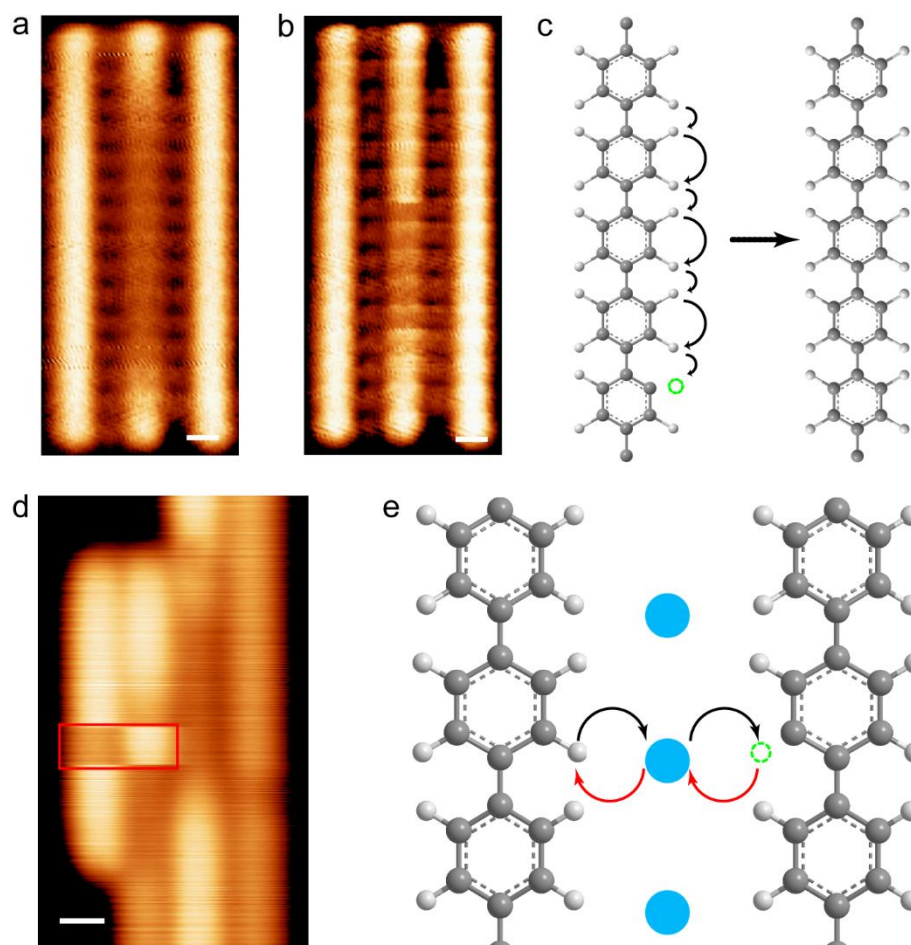
Figure S9. Proposed mechanism for inter- and intra-chain hopping. a-b. STM images showing the intra-chain hopping (a. Bias: 0.5 V, Current: 20 pA, Scale bar: 0.5 nm; b. Bias: -0.1 V, Current: 30 pA, Scale bar: 0.5 nm). **c.** The proposed intra-chain hopping model: concrete proton tunneling along the edge. **d.** STM image showing a reversible inter-chain hopping process (Bias: 1 V, Current: 10 pA, Scale bar: 1.0 nm). **e.** The proposed inter-chain hopping model: indirect proton tunneling via a Br atom (blue dot).

REFERENCES

(1)   Porezag, D.; Frauenheim, Th.; Köhler, Th.; Seifert, G.; Kaschner, R. Construction of Tight-Binding-like Potentials on the Basis of Density-Functional Theory: Application to Carbon. *Phys. Rev. B* **1995**, *51* (19), 12947–12957.

(2)   Son, Y.-W.; Cohen, M. L.; Louie, S. G. Energy Gaps in Graphene Nanoribbons. *Phys. Rev. Lett.* **2006**, *97* (21), 216803.

(3)   Blöchl, P. E. Projector Augmented-Wave Method. *Phys. Rev. B* **1994**, *50* (24), 17953.

(4)   Kresse, G.; Joubert, D. From Ultrasoft Pseudopotentials to the Projector Augmented-Wave Method. *Phys. Rev. B* **1999**, *59* (3), 1758.

(5)   Kresse, G.; Furthmüller, J. Efficiency of Ab-Initio Total Energy Calculations for Metals and Semiconductors Using a Plane-Wave Basis Set. *Comput. Mater. Sci.* **1996**, *6* (1), 15.

(6)   Kresse, G.; Furthmüller, J. Efficient Iterative Schemes for Ab Initio Total-Energy Calculations Using a Plane-Wave Basis Set. *Phys. Rev. B* **1996**, *54* (16), 11169.

(7)   Hammer, B.; Hansen, L. B.; Nørskov, J. K. Improved Adsorption Energetics within Density-Functional Theory Using Revised Perdew-Burke-Ernzerhof Functionals. *Phys. Rev. B* **1999**, *59* (11), 7413.

(8)   Grimme, S.; Antony, J.; Ehrlich, S.; Krieg, H. A Consistent and Accurate Ab Initio Parametrization of Density Functional Dispersion Correction (DFT-D) for the 94 Elements H-Pu. *J. Chem. Phys.* **2010**, *132* (15), 154104.

(9)   Ji, W.; Lu, Z.-Y.; Gao, H. Electron Core-Hole Interaction and Its Induced Ionic Structural Relaxation in Molecular Systems under X-Ray Irradiation. *Phys. Rev. Lett.* **2006**, *97* (24), 246101.

(10)   Wang, C.; Zhou, X.; Pan, Y.; Qiao, J.; Kong, X.; Kaun, C.-C.; Ji, W. Layer and Doping Tunable Ferromagnetic Order in Two-Dimensional CrS_2 Layers. *Phys. Rev. B* **2018**, *97* (24), 245409.